Chemistry–A European Journal
Research Article
doi.org/10.1002/chem.202202249
Chemistry Europe
European Chemical Societies Publishing

www.chemeurj.org

Probing the Structural Dynamics of a Bacterial Chaperone in Its Native Environment by Nitroxide-Based EPR Spectroscopy

Annalisa Pierro,[a, b] Alessio Bonucci,[a] Davide Normanno,[c, d] Mireille Ansaldi,[e] Eric Pilet,[a] Olivier Ouari,[f] Bruno Guigliarelli,[a] Emilien Etienne,[a] Guillaume Gerbaud,[a] Axel Magalon,[e] Valérie Belle,[a] and Elisabetta Mileo*[a]

Abstract: One of the greatest current challenges in structural biology is to study protein dynamics over a wide range of timescales in complex environments, such as the cell. Among magnetic resonances suitable for this approach, electron paramagnetic resonance spectroscopy coupled to site-directed spin labeling (SDSL-EPR) has emerged as a promising tool to study protein local dynamics and conformational ensembles. In this work, we exploit the sensitivity of nitroxide labels to report protein local dynamics at room temperature. We demonstrate that such studies can be performed while preserving both the integrity of the cells and the activity of the protein under investigation. Using this approach, we studied the structural dynamics of the chaperone NarJ in its natural host, *Escherichia coli*. We established that spin-labeled NarJ is active inside the cell. We showed that the cellular medium affects NarJ structural dynamics in a site-specific way, while the structural flexibility of the protein is maintained. Finally, we present and discuss data on the time-resolved dynamics of NarJ in cellular context.

Introduction

"Cellular structural biology" approaches are emerging with the common aim of exploring biomolecule structures and interactions directly under physiological conditions.[1] As the cellular environment cannot be reproduced in vitro, the investigation of biomolecules directly inside cells has attracted a growing interest in the past decades. This exciting trend currently embraces different techniques, including cryo-electron tomography,[2] crosslinking mass spectrometry,[3] FRET spectroscopy,[4] computational modeling[5] and magnetic resonances techniques.[1,6] Among these last, electron paramagnetic resonance (EPR) spectroscopy coupled with the use of paramagnetic labels (site-directed spin labeling approach, SDSL) has shown to be very appealing in following protein structural dynamics and conformational changes within the context of the cell.[7] Since 2010 and the first in-cell article by Tochio and Shirakawa,[8] significant progress has been made in this field. Based on the introduction of paramagnetic labels into a biomolecule of interest, at user-defined sites, the SDSL-EPR approach is a valuable and manifold tool offering competitive advantages for in-cell structural studies, thanks to the negligible background interference from other cellular components, the accessible timescale window (from ns to μs), its high sensitivity (few μL at few μM concentration), and no molecular size limit of the biomolecule under study.[9,45]

To date, with the exception of a study focused on the stability of a dimeric protein in HeLa cells,[10] the research in the field of in-cell EPR has been mainly focused on the development of spin labels characterized by enhanced features for cellular studies,[11] on the development and establishment of

[a] *Dr. A. Pierro, Dr. A. Bonucci, Dr. E. Pilet, Prof. B. Guigliarelli, Dr. E. Etienne, Dr. G. Gerbaud, Prof. V. Belle, Dr. E. Mileo*
Aix Marseille Univ, CNRS, BIP
Bioénérgetique et Ingénierie des Protéines, IMM
13009 Marseille (France)
E-mail: emileo@imm.cnrs.fr

[b] *Dr. A. Pierro*
Department of Chemistry, University of Konstanz, and Konstanz Research School Chemical Biology,
78457 Konstanz (Germany)

[c] *Dr. D. Normanno*
Aix Marseille Univ, CNRS, Inserm
Institut Paoli-Calmettes, CRCM
Centre de Recherche en Cancérologie de Marseille
13273Marseille (France)

[d] *Dr. D. Normanno*
Univ Montpellier, CNRS, IGH
Institut de Génétique Humaine
34396 Montpellier (France)

[e] *Dr. M. Ansaldi, Dr. A. Magalon*
Aix Marseille Univ, CNRS, LCB
Laboratoire de Chimie Bacterienne, IMM
13009 Marseille (France)

[f] *Prof. O. Ouari*
Aix Marseille Univ, CNRS, ICR
Institut de Chimie Radicalaire
13397 Marseille (France)

Supporting information for this article is available on the WWW under https://doi.org/10.1002/chem.202202249

suitable methodologies[12] and on the proof of the feasibility of this kind of approach. In particular, the majority of the published in-cell EPR studies is based on DEER experiments,[10,11c,e,12c,13] which involve the grafting of two paramagnetic labels into specific positions of a protein and on measurements of distance distributions between them. DEER experiments enable to probe the global structure and possible conformations of the protein under investigation.[14] As a consequence of the relaxation properties of the spin labels currently available, DEER measurements are carried out on frozen samples (typically 10–60 K).

The possibility of running EPR investigations of protein structural dynamics at room temperature is of high interest in the context of cellular studies. Preserving the health and the metabolic activity of the cells under investigation is indeed a key point for more relevant data on local structural dynamics.

Among the spin labels currently available, nitroxides are the only ones allowing SDSL-EPR studies of proteins at room temperature and in solution by continuous wave EPR measurements (CW-EPR). This is mainly related to the fact that the EPR spectrum of nitroxides contains information not only about magnetic interactions but about molecular dynamics, as well.[15] Indeed, the CW-EPR spectrum of a nitroxide grafted to a protein reports on the structural properties of the protein under investigation and, for example, can be used to follow structural and folding changes and to detect interaction sites in complexes.[16] Despite the appealing perspective offered by nitroxide labels, the possibility of running in-cell EPR studies under physiological conditions is still very poorly investigated and under-exploited. At present, only three works, applying room temperature EPR spectroscopy on proteins delivered in cell have been reported.[17] Two of them investigate the structural dynamics of the human alpha-synuclein[17a] and of immunoglobulin binding domain of protein G (GB1),[17c] respectively, microinjected in *Xenopus laevis* oocytes, while the other focuses on the intracellular delivery of proteins by heat-shock.[17b] Additional examples were given by in-situ EPR studies.[18] Indeed, this approach to study membrane proteins in their cellular environment at physiological temperature, currently developed in the groups of Cafiso[20] and Joseph,[21] is achieved by labeling extracellular regions of membrane proteins directly on cell suspension. However, such kind of experiments, specific for membrane proteins, evidently differs from those used for in-cell EPR studies.

Our work aims at demonstrating the ability of nitroxide labels in reporting on structural dynamics of cytosolic proteins in their native environment, in experiments carried out at room temperature. This approach offering the appealing possibility of observing cellular events in real time at room temperature.

In particular, we focused on the investigation of a bacterial protein, NarJ, within its cellular environment. NarJ is a cytosolic chaperone from *Escherichia coli* that ensures folding and assembly of the membrane-bound-respiratory nitrate reductase complex, NarGHI, member of a large group of molybdenum-containing enzymes.[22]

In-cell experiments were performed on in-vitro-labeled proteins delivered in cells by electroporation. The efficiency of delivery and the correct localization of NarJ was firstly confirmed by fluorescence microscopy, flow cytometry and EPR investigation of the functional integrity of the delivered protein, designing a NarJ-specific activity assay carried out on whole cells. Finally, from the EPR investigation of five different labeled variants of NarJ in dilute buffer solution, in cell lysate and in whole cells, we were able to show i) that structural dynamics of NarJ in the cytosol drastically differs from what observed in vitro and in cell lysates, ii) that the intracellular medium clearly affects NarJ structural dynamics in a site-specific way and iii) that these measurements were carried out in a time window which guarantees the viability of the cells under investigation. Finally, data on the time-resolved monitoring of NarJ protein in the cellular context will be presented and discussed.

Results

NarJ, a cytosol chaperone from *E. coli*: Variants design and in-vitro studies

In order to investigate the impact of the intracellular environment on NarJ structural dynamics, the spin label maleimido-Proxyl (**1**, Figure 1B) was grafted to Cys residues introduced by site-directed mutagenesis at several positions of NarJ, as depicted in Figure 1A. For the choice of labeling positions, we exploited structural data currently available for NarJ (P0AF26), allowing the identification of a globular domain (gray in Figure 1), mostly composed of helices and flexible regions. This domain includes a highly conserved hydrophobic cavity, involved in partner recognition which NarJ assists in concerted folding upon insertion of metal centers.[23] The region encompassing the last 50 aa (in magenta in Figure 1), which we will refer to as the C-ter region, is a less conserved region among NarJ homologues and it exhibits a flexible structural behavior.[24] The unique natural Cys residue (C207) located in the "C-ter

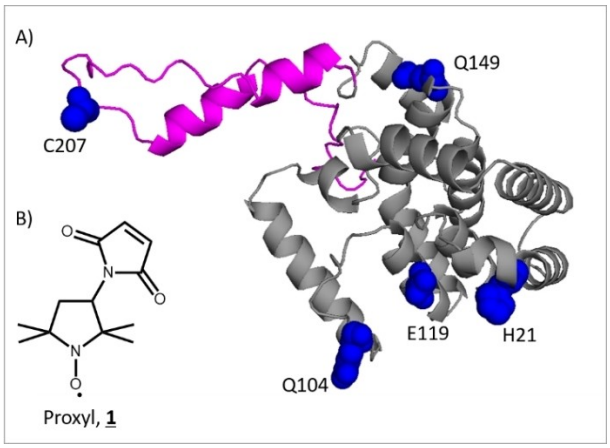

Figure 1. A) Model structure of NarJ (P0AF26) from AlphaFold.[19] The blue spheres indicate the amino acids targeted for Cys mutation and labeling. The structural segment in magenta correspond to the C-ter region. B) Chemical structure of the spin label used in this work.

region" is one of the labeled sites. Then, other single Cys variants, were generated on a truncated form of NarJ (NarJT), lacking the C-ter region. The description of the functionality of the truncated protein was made by Magalon's team;[23a] the corresponding NarJT protein proved to be a valuable construct for studying the molecular mechanism of metalloprotein partner recognition and binding because its binding parameters remained constant. Thus, various regions were targeted on NarJT: E119C, located in a hydrophobic groove, H21C and Q104C, located on either side of this groove, and Q149C is in a region opposite to the cavity. An additional variant, containing two Cys residues (H21C/Q104C) for double labeling and distance measurements, was also prepared. As for previous studies,[11a,23b] all the variants were labeled with Proxyl (**1**) with labeling yields equal or higher than 90%.

The EPR spectra of all NarJ variants in dilute solution are shown in Figure 2A–E. All the experimental data were simulated with SimLabel[25] (a GUI of EasySpin[26]) using a minimum of two components characterized by different rotational correlation times, τ_c, with the unique exception of position Q149C, for which only one component was employed. The τ_c is the parameter related to the local mobility of the nitroxide, the lower this value, the higher the mobility. In the plots resuming simulation results (Figure 2K–O), we refer to the component with the lower τ_c as sharp and to the one with higher τ_c as broad. Simulation parameters are reported in the Supporting Information. In dilute buffer solution, the labeling sites of NarJ show increasing label dynamics as follows E119C < H21C < Q149C < Q104C < C207 consistent with data we have already reported.[11a,23b]

NarJ protein is efficiently delivered inside *E. coli* cells through electroporation

Inspired by the work of Kapanidis and collaborators,[27] we optimized a method based on electroporation to deliver exogenously labeled NarJ inside its natural host, *E. coli* cells. The experimental protocol, detailed in M&M and in supporting material (Figures S1 and S2 in the Supporting Information), consists in applying an electric shock on a cell suspension, previously incubated for 10 minutes with a solution containing the labeled protein. After electroporation, the non-internalized proteins are washed away and the cell sample is resuspended in the most appropriate medium before EPR measurements. To investigate the proper NarJ internalization, we combined EPR spectroscopy, laser scanning confocal microscopy (LSCM) and flow cytometry (FC). In the case of LSCM and CF studies, NarJ was labeled with a fluorophore.

Figure 3A shows the EPR spectrum obtained for cells incubated with the spin-labeled protein (NarJ variant Q149C^{Proxyl}) but not subjected to electroporation: no significant EPR signal is visible (blue trace, Figure 3A) whereas a EPR signal is obtained for cells that had been electroporated (black trace, Figure 3A).

To further investigate the effective delivery of NarJ into cells we performed 3D LSCM imaging in Airyscan modality to achieve improved resolution and volumetric information. NarJ labeled with the organic dye Cy5 was incubated with the cells and either washed out or delivered to cells employing the same electroporation protocol and conditions than those used for EPR measurements.

Fluorescence images of non-electroporated cells ("in contact" sample) showed a faint signal almost indistinguishable from the background (Figure 3B) whereas, after electroporation, a strong specific signal was associated with the cells, indicating that NarJ has been internalized in the cytosol of bacteria

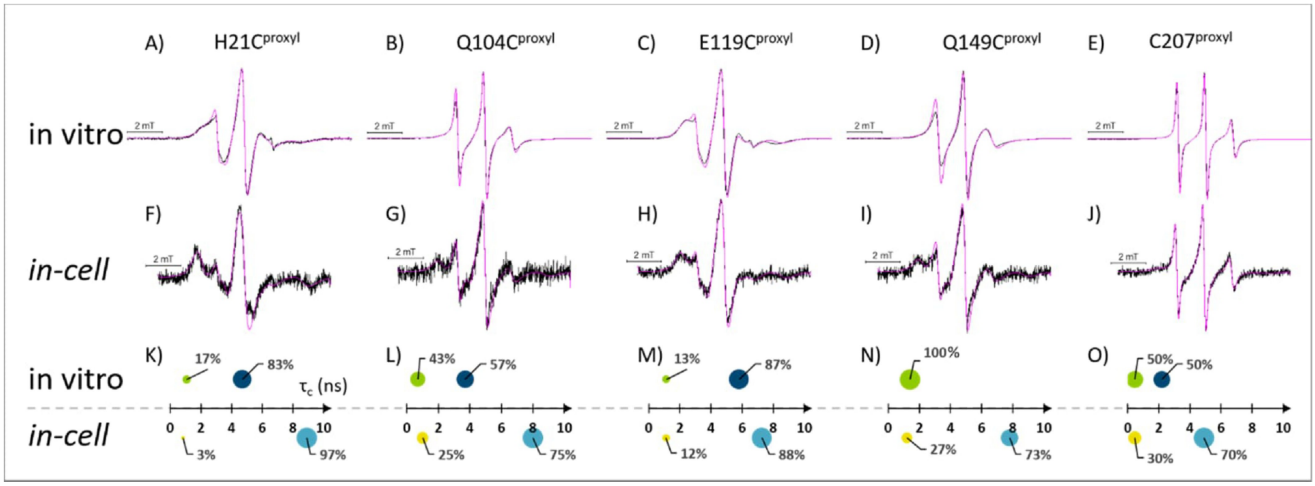

Figure 2. Room-temperature, X-band CW-EPR spectra recorded for the studied NarJT variants and NarJ labeled with Proxyl in vitro (1 scan in Tris buffer 10 mM, pH 7.4, A–E) and in *E. coli* cells (10 scans, 15 minutes' acquisition time, F–J). Experimental data are in black; simulated ones are in magenta. K–O: τ_c extracted from the simulations using SimLabel are plotted on the *x*-axis: the percentage of each population described by a τ_c is represented as a surface of a green or navy disc for in vitro data, or yellow or sky blue for in-cell.

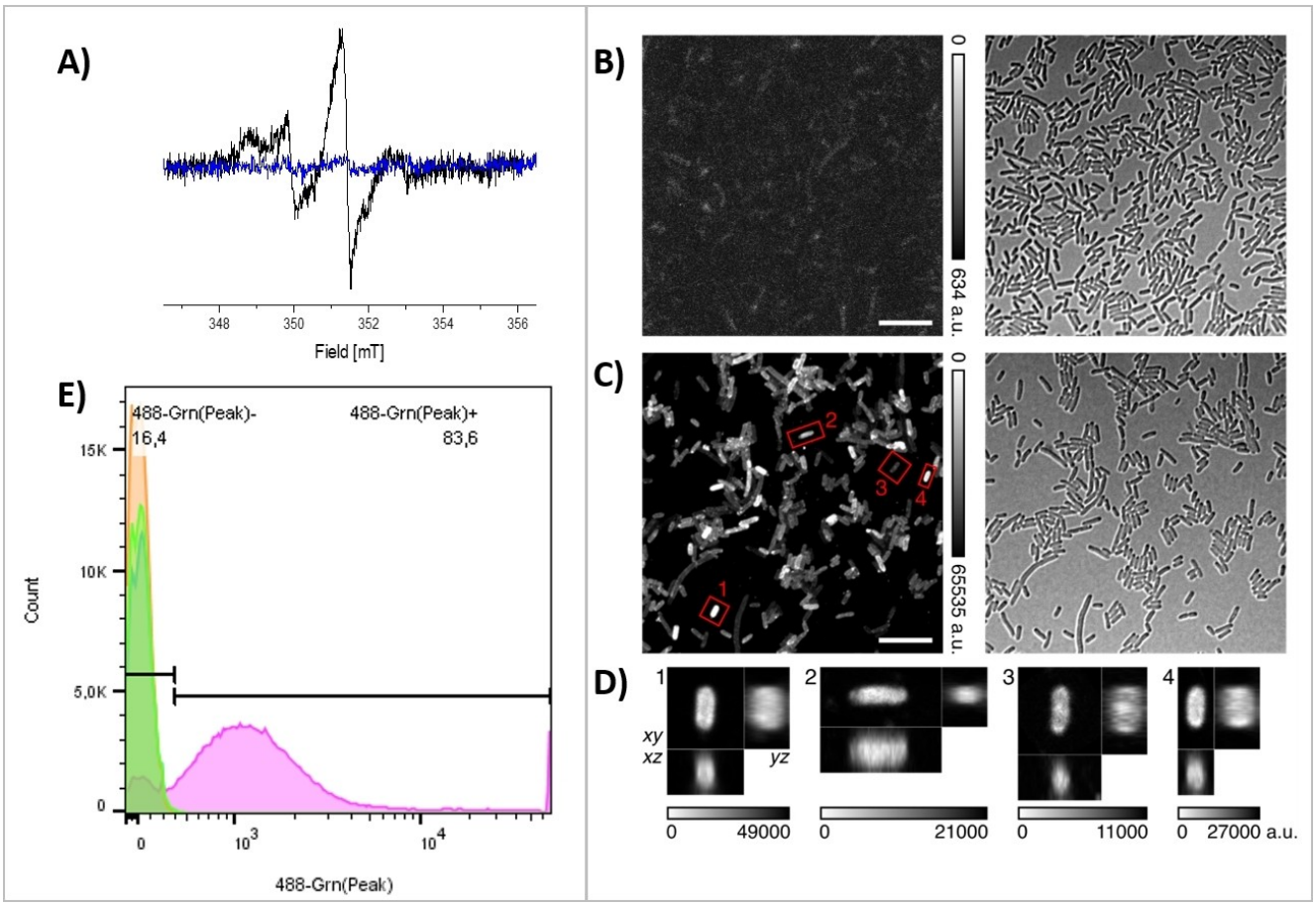

Figure 3. A) Blue trace: room-temperature CW-EPR spectrum of a cell sample "in contact" with the labeled protein NarJT-Q149C but not electroporated. Black trace: room temperature CW-EPR spectrum of the same protein delivered inside *E. coli* cells by electroporation. B) Fluorescence (left) and transmission (right) images of NarJ-Cy5 "in contact" with bacteria but not electroporated. The fluorescence image shows a maximum intensity projection (MIP) of a *z*-stack, while the transmission image corresponds to a single plane acquired in DIC mode. C) Fluorescence (MIP, left) and transmission (DIC, right) images of NarJ-Cy5 electroporated bacteria. D) Examples of *xy*, *xz*, and *yz* sections of the regions indicated in red in (C) for cells having internalized varying quantities of NarJ-Cy5. Scale bars: 10 μm. E) Fluorescence intensities of electroporated bacterial populations measured by flow cytometry. Cytometry histograms represent the number of fluorescent or nonfluorescent cells gated to the bacterial population as a function of the fluorescence intensity, percentages of the populations are also indicated. The limit between negative (488-Grn(Peak)-) and positive fluorescence (488-Grn(Peak) +) was determined by the fluorescent-negative non-electroporated control. Color code: non-electroporated cells: orange, H_2O electroporated cells: blue, fluorescently-labeled NarJ incubated with non-electroporated cells (green), fluorescently-labeled-NarJ incubated with electroporated cells (pink).

(Figure 3C). Importantly, the absence of fluorescence signal in not electroporated cells suggests that the protein does not stick to the bacterial outer membrane in a nonspecific manner and that the washing cycles are effective at removing non-internalized protein. Further imaging experiments confirmed that results are robust with respect to the organic dye used to label NarJ; that electroporation per se does not induce fluorescence; that washout cycles completely remove free protein from solution (Figure S3). Orthogonal views analysis of the 3D images of electroporated cells (Figure 3D) shows a uniform internal distribution of NarJ-Cy5 in the bacteria, irrespectively of the quantity of protein internalized (i.e., the fluorescence intensity of the cell). Furthermore, as visible in Figure 3B and C, right, electroporated cells are indistinguishable from non-electroporated ones, which suggests that the delivery protocol does not affect cell physiology.

In order to accurately quantify the proportion of cells that incorporate NarJ upon electroporation, we performed flow cytometry experiments using fluorescently labeled protein.

Such an analysis presents the advantage to rely on a large number of cells (over 300 000 cells in the experiments reported here). Figure 3E indicates that a large proportion of cells ranging from 82 to 93 % depending on the specific experimental replica, showed fluorescence after electroporation with fluorescently-labeled NarJ when compared to cells that were not electroporated ("in contact") or were electroporated with unlabeled NarJ.

Furthermore, to investigate the possibility of leaking out of the protein, after in-cell delivery, samples were left for ~1 h at room temperature.

After centrifugation, the supernatant was checked by EPR. The absence of a signal confirmed that no protein was released outside the cell during 1 h (Figure S4), ~4 times longer than the

time used to average the spectra presented in this work (10 scans, 15 min). To determine if during this 15 minutes' time window, cell viability is modified, serial dilution of electroporated (Figure S5A) and non-electroporated (Figure S5B) *E. coli* cells onto LB agar plates were carried out after incubation in PBS buffer for different time intervals. Our experiment showed that both cell samples are viable in PBS buffer over an interval of 25 minutes. After this time, we highlighted a slow decrease of the duplication ability, symptom of cell sufferance and starvation. It is worth noticing that the time needed to prepare an in-cell sample is between 10–15 min (see the Experimental Section), so that the end of the 15 min EPR recording fits the duration of cell viability.

Taken together, all these results show that our electroporation-based method can be used to successfully deliver cytosol-diffusing labeled-NarJ proteins into *E. coli* cells.

Electroporated NarJ reaches the bacterial cytosol in an active and functional state

After validation of the delivery of NarJ inside bacteria, we addressed the point if electroporated NarJ is still functional and able to interact with its biological partners. The functionality of NarJ was evaluated by performing an activity test on an intact cell suspension, monitoring the nitrate reductase activity of the NarGH subunit.[28] Indeed, NarJ is an essential chaperone in the activation of the NarGH catalytic dimer through the acquisition of metal centers.[22b,c] Thus, if NarJ is not present, the NarGH subunit is inactive and unable to reduce nitrate.

The activity test consists in delivering NarJ (labeled or not) by electroporation in cells overexpressing apo-NarGH, the inactive form of the enzyme, soluble in the cytosol. The enzyme activation was monitored by measuring the nitrate reductase activity. As demonstrated previously, in absence of the membrane-anchor NarI subunit, the soluble and cytoplasmic NarGH complex displays nitrate reductase activity using reduced benzyl viologen (BV) as an artificial electron donor.[22c] The reduced form of BV (BV^{red}) has a bright blue-violet color, absorbing at 604 nm, and it can diffuse freely through the membranes (Figure 4A).[29]

Nitrate transport across biological membranes is facilitated by two ATP-independent nitrate/nitrite transport proteins NarK and NarU in *E. coli*.[30]

Exogenous addition of BV^{red} and nitrate to NarJ-electroporated cells expressing immature NarGH complex is expected to exhibit activity as measured by loss of absorbance at 604 nm, that is, nitrate-dependent BV oxidation. To avoid nonspecific reduction of nitrate, we used a cell strain deficient of all the native nitrate reductases and their respective chaperones (Δ*narA*, Δ*nap*, Δ*narZ*, Δ*narJ*, Δ*narW*). All the samples were prepared as indicated in the M&M and the activity essays were performed in a glove box, under anaerobic conditions (95% N_2, 5% H_2). Cells expressing *narGHJ* genes produce a fully mature and active NarGH complex (holo-NarGH) and were used as positive control. A high and specific nitrate reductase activity was measured in those cells as compared to cells expressing

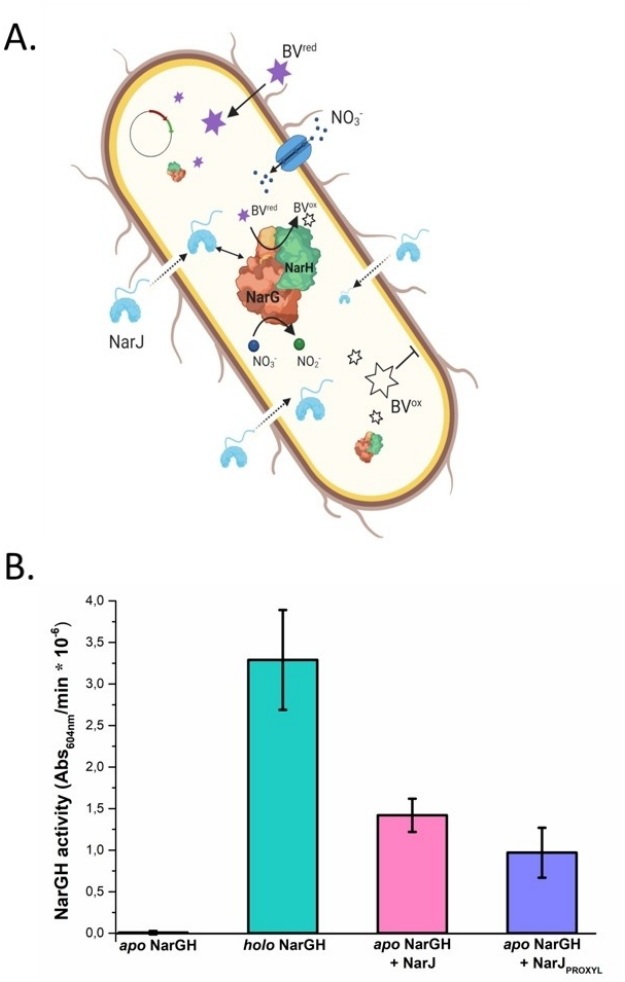

Figure 4. A) Schematic illustration of the in-cell enzymatic assay optimized to follow NarJ activity in *E. coli* cells. B) NarGH activity measured through the oxidation of BV: cells overexpressing apo-NarGH (negative control), holo-NarGH (positive control, green), apo-NarGH (in which unlabeled NarJ was delivered, pink), apo-NarGH (in which labeled NarJ–C207 was delivered, purple). The error bars were calculated as the standard error on six replicates of each experiment. Created with BioRender.com.

only allowed the detection of a significant activity. A similar result was obtained also by delivering a labeled variant of NarJ (NarJ-C207). In conclusion, these results indicate that electroporated NarJ reaches the cytosol in an intact, functional state and is, thus, able to restore the NarGH activity even when labeled with a nitroxide spin label.

NarJ structural dynamics behavior under cell conditions at room temperature

Electroporation of spin-labeled NarJ and EPR measurements are compatible with cell viability

To address the question of how the intracellular medium modulates NarJ local structural dynamics, NarJ variants were individually delivered in *E. coli* cells and the EPR signal was

acquired over 15 minutes at room temperature. This time window, corresponding to the real time the sample spent in the EPR cavity, was chosen because it resulted a good compromise between the intracellular spin concentration, cell viability and an adequate signal-to-noise ratio of the EPR spectra. Indeed, regarding the spin concentration (bulk) of the in-cell experiments reported in this work, the delivery allowed to achieve a range between 7 and 11 μM. Interestingly, our results clearly show that the cells have a maximum of viability of 25 minutes in PBS/agarose and at room temperature (Figure S5), thus the time window used for in-cell EPR acquisition (15 min) is compatible with *E. coli* cells viability.

The intracellular medium affects NarJ local dynamics

Figure 2F–J shows the EPR spectra obtained by delivering all the labelled NarJ variants in *E. coli* cells. A first visual inspection reveals that spectra of in-cell samples are broader respect those obtained in vitro, reporting a decrease in the mobility of the nitroxide in this environment. This finding could be compatible with a gain in protein folding and in its structural compactness. As shown in Figure S6, these spectral shapes were reproducible in biological replicates. For a deeper investigation, all the EPR spectra showed in Figure 2 were simulated with SimLabel.[25] In the simulation plots (Figures 2K–O and S7), we refer to the component with the lower τ_c as sharp and to the one with the higher τ_c as broad. Complete simulations parameters are reported in the Supporting Information. The EPR spectrum of Proxyl grafted in the hydrophobic cavity of NarJ (position 119), is poorly affected by the cellular environment, with the ratio of components being unaltered. The increase of the value of τ_c of the broad component is particularly drastic for position 21, 104 and 149, for which also the weight of this population increases. Notably, position H21C exhibits an increase by over 90%, of τ_c going from ~5 ns in vitro to ~9 ns in cell, this last being the higher τ_c obtained in this study. For positions Q104C and Q149C, the broad component characterized by a τ_c of ~8 ns, becomes predominant in intracellular condition. It is important to highlight that position Q149C is the most affected one, characterized by the higher increase in the value of the τ_c compared to the other positions (Figure S7). Intermediate behavior between the cases mentioned above has been detected for the label grafted to position C207.

With a moderate increase of the broad component both in weight and in τ_c, this region maintains the higher degree of flexibility inside the cell.

Besides showing that the structural dynamics of NarJ observed in-cell is different from that protein shows in the dilute buffer solution, these findings demonstrate that the intracellular environment affects NarJ structural dynamics in a site-specific fashion.

Mimicking the cytosol with crowders and cell lysates

Crowding agents are currently used by scientists to recreate simpler environments than those of in-cell experiments but more complex than in vitro ones, with the aim of deciphering in-cell data.[13d,31]

In particular, in this study we chose to use: sucrose, an osmolyte sequestrating water molecules in the surrounding of the protein;[32] potassium glutamate (KGlu), the most abundant potassium salt in *E. coli*;[33] BSA, representing charged globular proteins[34] and Ficoll a polymer used to simulate excluded volume effects of the cytoplasm.[35] Figure 5 shows the EPR spectra obtained in the presence of crowders, while Figure S8 resumes the results of the simulations. As a general trend, BSA, Ficoll and sucrose were the additives affecting the most NarJ structural dynamics with variants H21C and Q104C being the most sensitive sites and showing spectral changes similar to those observed in cell. In the case of the wild type protein, the position C207 was sensitive uniquely to the presence of Ficoll, which induces spectral changes very similar to those obtained in cell. In the case of position E119C, spectral variations were detected in the presence of BSA, Ficoll and sucrose but are smaller than those observed in cell. Unexpectedly, position Q149C, which mobility was strongly affected by the cytosol, showed very small sensitiveness to all the crowders employed in this study.

Cell lysates are also currently used to try to decipher results obtained by in-cell studies, being considered a step towards more biologically relevant crowders.[36] The EPR spectra obtained by solubilizing NarJ variants in *E. coli* lysates are showed in Figure S9 and are very similar to those obtained in vitro. The only difference we observed between the experiments carried out in cell lysates and in whole cells concerned the reduction of the nitroxide, which was much faster in lysates

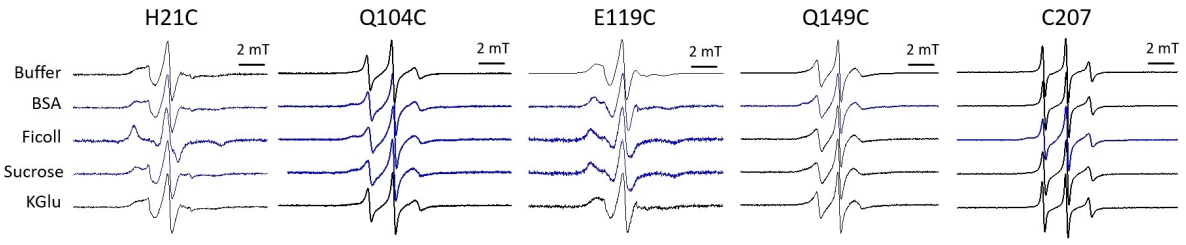

Figure 5. Room-temperature, X-band CW-EPR spectra for the studied NarJT variants and NarJ labeled with Proxyl in vitro (Tris buffer 10 mM, pH 7.4) and in the presence of crowding agents (BSA 300 mg mL ^{1}, Ficoll-70 300 mg mL ^{1}, Sucrose 30% *w/v* and potassium glutamate (KGlu) 200 mM). If changes are detected upon adding crowding agent, spectra are shown in blue.

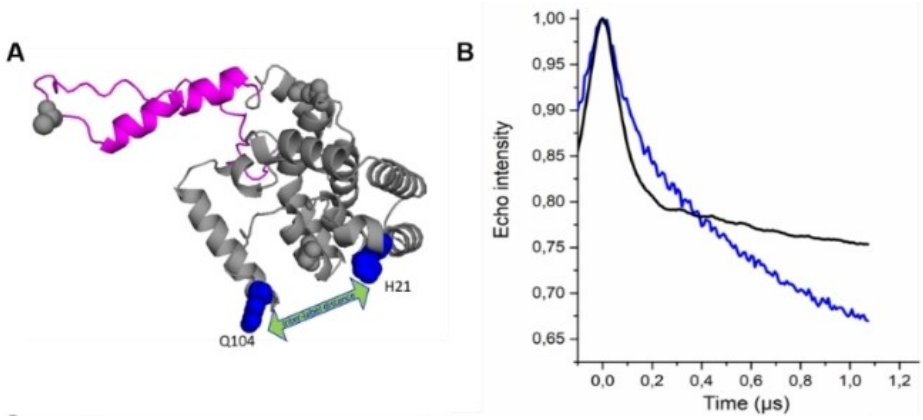

Figure 6. A) Structural model of NarJ indicating the labeled positions. B) Q-band 60 K raw DEER data obtained in vitro (black) and in *E. coli* cells (blue).

than in whole cells (Figures S10 and S13, respectively). Indeed, as showed in Figure S10, after 10 minutes in cell lysates, the signal of C207^{Proxyl} is completely reduced, while in whole cells a decay of 50% of the EPR signal is observed after ~300 minutes (Figure S13, green curve).

In-cell DEER

In previous works, we demonstrated that NarJ shows a high structural flexibility in dilute buffer solution[23b] and that such flexibility is maintained in model cells (*X. laevis* oocytes).[11a] At this point we aimed at investigating the impact of the native cellular environment, *E. coli*, on NarJ. The doubly-labeled NarJ variant, H21C/Q104C, was used to measure distance distributions between the two spin centers in-cell by DEER experiments performed at Q-band. The positions H21 and Q104 (Figure 6A) were selected because they revealed a conformational change when NarJ interacts with its biological partner, the NarGH complex.[7,23b] The in-cell sample was prepared by delivering the doubly labeled variant inside *E. coli* cells as previously described in the text for singly labeled variants. ~15 minutes after delivery, the sample was shock-frozen in liquid nitrogen to perform DEER experiments at 60 K.

Figure S11 shows the echo-detected field sweep (EDFS) of the *E. coli* cell sample versus a sample in which the protein and the cells were put in contact and no electric pulse was applied. For non electroporated samples, no EPR signal is detectable at the temperature of EDFS acquisition (60 K), unlike the electroporated one. Echo decay curves are shown in Figure S12 and phase memory times (T_M) are ~4 and ~1 µs, for the in vitro and the in-cell sample, respectively. As the T_M is mainly driven by the coupling of the spin centers with the nuclei nearby and by spin diffusion, the shortening of the T_M in cells can be attributed to the high concentration of ^{1}H in this environment. As a consequence, in-cell DEER data were collected for a too short evolution time (1 µs) to unambiguously determine the background and derive reliable distance profiles.[14b]

EPR time-resolved monitoring of NarJ variants in *E. coli*

As a perspective of this work, we were interested in investigating the EPR signatures of NarJ in-cell at room temperature over time.

To this aim we extended the time window for data acquisition beyond 15 minutes and monitored the integral of the EPR spectra of all NarJ variants over 16 h under cellular conditions. The results are shown in Figure 7 and all the NarJ variants show a time-dependent decrease in the signal intensity. This expected trend is related to the reduction of the nitroxide to a diamagnetic species (hydroxylamine) under the action of antioxidants and enzymes present inside the cytoplasm, which results in the decrease of the EPR signal intensity over time.[11a,37] Note that the differences observed in the reduction profiles are related to different degrees of accessibility of reductant with respect to the position in which the label is grafted. Then, we investigated the EPR peak-to-peak amplitude of the central line of the EPR spectra of all NarJ variants at room temperature over time. All the data are shown in Figures 8 and S15. In particular, while for position H21C a

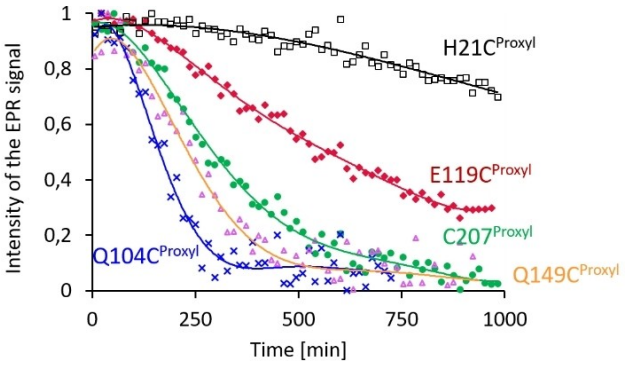

Figure 7. Normalized integrated intensity of the EPR spectra of all NarJ variants in *E. coli*. H21C: black, E119C: red, C207: green, Q149C: magenta, and Q104C: blue. Each point represents the sum of the integrated intensity of 10 consecutive EPR spectra.

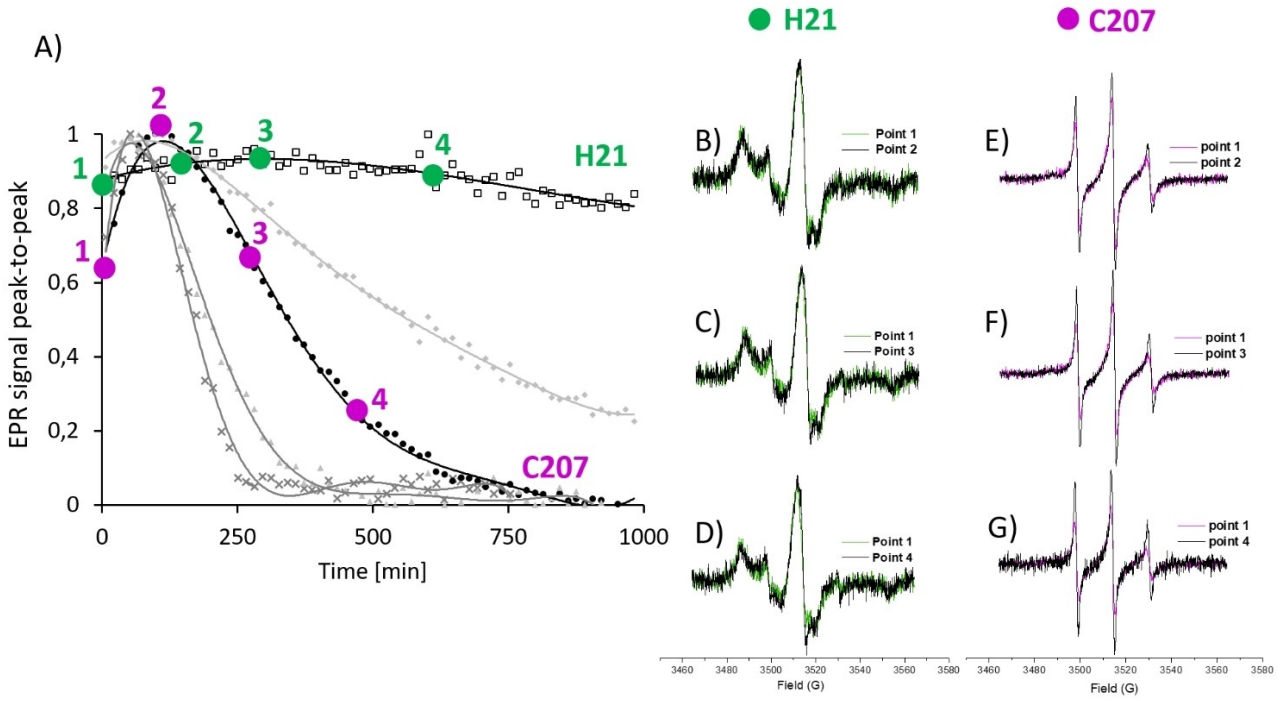

Figure 8. A) Peak-to-peak (h_0) profiles of C207^{Proxyl} and H21C^{Proxyl} NarJ variants in *E. coli* cells are indicated as black curves. The points from which the EPR spectra are extracted are highlighted in color (magenta for C207 and green for H21). Profiles of the other variants are represented in gray. Superposition of CW EPR spectra corresponding to the points indicated on the curves in (A) for B) points 1 and 2 of variant H21C; C) points 1 and 3 of H21C; D) points 1 and 4 of H21C; E) points 1 and 2 of C207; F) points 1 and 3 of C207; and G) points 1 and 4 of C207. Each point represents the sum of the peak-to-peak intensity of 10 consecutive EPR spectra. Each spectrum showed in (B) to (G) has been normalized to its integrated intensity.

progress decrease in the peak-to-peak value is observed over time, for the other positions peak-to-peak values increase before starting to decrease more steeply. This behavior is surprising, because, in the light of the known reduction of nitroxides to EPR silent hydroxylamines in the cellular environment, a decrease in the peak-to-peak amplitude was expected for all the monitored positions.

Indeed, we addressed the point of possible variations of cell and protein concentration. Particular attention was made in the preparation of cell samples, which were performed using the same cell batch and the same cell dilution. This gave a *bulk* spin concentration between 7 and 11 μM for all the variants studied. Moreover, to avoid variation in the recorded signals related to cell sedimentation in the EPR capillary over time (Figure S14), cells were suspended in a buffer containing agarose.[38] Indeed, the differences observed in the curves are not related to a difference in the number of cells or spin concentrations used for experiments.

In order to better investigate possible changes in the spectral shapes, and thus in the nitroxide mobility, in Figure 8 we focus on the profiles obtained for one variant showing an increase of the peak-to-peak intensity (C207) and position H21, for which this phenomenon was not observed (Figure 8A). The superimposition of the EPR spectra corresponding to different times, respect to the first acquired spectrum, obtained for position H21 (green spots in Figure 8A) and for C207 (magenta spots in Figure 8A) are shown in Figure 8B–D and E–G, respectively: while the EPR lineshape for position H21C does not change over time, for position C207 the spectral lineshape becomes sharper. In order to avoid variations in the spin concentration, due to reduction in the cytosol, each selected spectrum from the kinetic curves (in Figure 8 for positions 207 and 21 and Figure S15 for the other positions) was normalized for its integrated intensity. Comparisons between the spectra at different times of the curves clearly show that a sharpening of the EPR spectra occurs with time for position 207, 104 and to a lesser extent for 119, while positions 21 and 149 are not affected. We can conclude that the sharpening observed for positions 207, 104 and 119 is related to an increase in the label mobility in the cytosol, which could be explained by the possible action of proteases or the unfolding of the protein structure.

Discussion

Here we report the results obtained by mapping the structural dynamics of NarJ, a cytosolic chaperone, in intact cells at room temperature combining nitroxide spin labels and EPR spectroscopy. To this aim, five NarJ variants, labeled with the spin label Proxyl at different regions of the protein, were delivered by electroporation in the natural host of the chaperone, *E. coli*. Even if electroporation has been extensively used to deliver proteins in different eukaryotic cell lines,[13a,b,39] in the case of

bacteria, the delivery is not straightforward, and fewer examples can be found in the literature. For this reason, we deeply investigated NarJ delivery by fluorescence microscopy and flow cytometry. Thanks to these last two approaches, we were able to demonstrate that NarJ delivery in *E. coli* cells is efficient and reproducible. Furthermore, fluorescence microscopy demonstrates that delivered NarJ proteins were homogeneously distributed in the bacterial cytosol. We also aimed at investigating the functional integrity of delivered NarJ. This chaperone has an essential role in the maturation of the NarGH enzyme, which, if active, shows nitrate reductase activity. A UV-Vis cellular activity test was implemented to monitor the nitrate reduction as a way to follow NarJ activity.

While no nitrate reductase activity was detected on a cell strain overproducing apo-NarGH complex, the electroporation-mediated delivery of exogenous NarJ in the same cell strain was able to restore the nitrate reductase activity. These results provide clear evidence that NarJ proteins remain active after delivery, as witnessed by their ability to complement the cell strain depleted in NarJ.

Afterward, we investigated the structural dynamics of NarJ in *E. coli* cells, by CW-EPR experiments at room temperature. Different degrees of broadening of the EPR spectra were observed compared to those monitored in diluted solution, with Q149C being the position characterized by the higher variation in the τ_c value, followed by H21C and Q104C. On the contrary, position E119, located in the conserved hydrophobic groove of NarJ, was only slightly affected. Position C207, which in vitro is characterized by a high flexible behavior, close to what was observed for IDPs, showed a τ_c variation higher than position E119 but drastically lower than what observed for the other positions. Even so, this region of the C-ter tail keeps a high flexibility, probably important for its biological role.

The observed decrease in nitroxide mobility, particularly evident for the protein core, could be explained with a gain in protein folding and/or in structural compactness compared to that in diluted solution. Indeed, similar local-dynamics changes have already been reported for soluble proteins subjected to conformational changes after the binding with a partner molecule but under in-vitro conditions.[46,47,48] Under our experimental conditions, the contribution of the main NarJ partner, the apo-NarGH complex, is negligible considering its very low expression level. Consequently the spectral changes we highlighted can be attributed to the cellular environment itself: unspecific attractive and/or repulsive interactions, volume exclusion effect in addition to the viscosity of the intracellular environment, which, for *E. coli*, is estimated to be three to eight times higher than that of water/buffer.[40]

Besides revealing that NarJ structural dynamics in cells differs from that observed in vitro, our results highlight a site-specific response of protein dynamics to the cytosolic environment. This finding suggests that the cytosol impact on NarJ structural dynamics is not a bulk, averaged effect. A position-dependent response of NarJ was also observed in presence of crowding agents, except for Q149C^{Proxyl} which was insensitive to the presence of all the crowding agents.

It is worth stressing that the time window for all the in-cell CW data shown (Figure 2) is 15 minutes thus it ensures the viability of the cells under investigation. Moreover, it is important to highlight that this time window is incredibly short with respect to the acquisition time currently needed for NMR spectra acquisition, that needs at least a couple of hours. To go further in this work and exploit all the advantages of room temperature studies, we reported a study focused on NarJ structural changes in cellular condition in a time-resolved fashion. Firstly, a site-specific reduction of nitroxide to hydroxylamine was observed and it was in agreement with the structural organization NarJ acquires in intracellular conditions. Then, by following the peak-to-peak amplitude of the central line of all the NarJ variants, we highlighted that only certain positions (Q104C, E119C and C207) are subjected to an increase in the peak-to-peak amplitude which revealed a sharpening of the EPR lineshape overtime. The latter is related to an increase in the mobility of the nitroxide label and, consequently, of the corresponding protein region. Protein degradation and unfolding are two possible explanations for this behavior. Indeed, the degradation of the protein by proteases would give a fragmentation of the protein and if the label is located on one of the generated peptides, its mobility will increase. The faster degradation of highly accessible regions, as demonstrated by limited-proteolysis coupled to mass spectrometry, could also explain the site-specific trend observed in the data here reported.[41] Protein unfolding during time inside cells was observed by NMR for several cytosolic proteins.[38b] In our case, the unfolding of a region in which the nitroxide is attached increases the spin label mobility and, as already mentioned, the sharpening of the signal. These hypotheses open the way for further investigations currently running.

Conclusion

Taken together, our work represents a leap forward in the development of EPR-based cellular structural biology that goes beyond the experimental feasibility. In particular, by exploiting nitroxide labels as reporters of protein local dynamics, we showed that SDSL coupled to EPR spectroscopy enables the investigation of protein structural dynamics in-cell at room temperature, under conditions ensuring the preservation of cell integrity. Moreover, based on the EPR study of NarJ protein in its host native cells, *E. coli*, we were able to show that structural dynamics of NarJ in the cytosol drastically differ from what was observed in vitro, and that the intracellular context clearly affects NarJ structural dynamics in a site-specific way. The value of these experimental findings is strengthened by assessing NarJ activity directly inside cells. Finally, we have demonstrated that nitroxides are suitable spin labels for studying the dynamic changes occurring inside cells in a time-resolved fashion.

Experimental Section

NarJ protein purification: Overexpression and purification of NarJ were carried out as described previously using a pET22b derivative vector carrying NarJT-6His or NarJwt-6His.[22a] The overexpression of all the variants was carried out in *E. coli* BL21(DE3) strain, growth in LB medium at 37 °C, induced by 0.2 mM of IPTG and incubated at the same temperature for 4 h. Cells from 1 L of culture are resuspended in 40 mL of Tris·HCl 50 mM pH 7.4 buffer, containing NaCl 150 mM and protease inhibitors EDTA free cocktail (Roche) and lysed by three passages into EmulsiFlex (Avestin) at 1500 psi. The resulting crude extract was centrifuged at 12000 *g* for 60 min. The resulting supernatant is, then, loaded in a Ni-NTA superflow columns 5 mL (Quiagen) previously equilibrated against Tris·HCl 50 mM pH 7.4, NaCl 300 mM, Imidazole 10 mM. The column is eluted against Tris·HCl 50 mM pH 7.4, NaCl 300 mM at three concentrations of Imidazole: 20, 50, and 200 mM, at which NarJ elutes. Fractions containing the protein are then dialyzed in a 3 kDa MWCO membrane against 500 mL Tris·HCl 50 mM pH 7.4, NaCl 150 mM for 2 h, renovating the buffer every 30 min.

Protein concentration was estimated using absorbance at 280 nm and an extinction coefficient of NarJ full length variants $\varepsilon_{280} = 21430\,M^{-1}cm^{-1}$ or NarJT variants $\varepsilon_{280} = 14400\,M^{-1}cm^{-1}$ (http://us.expasy.org/cgi-bin/protparam).

Cells strains and competence: The bacterial strains used in this study are listed in Table S17.

Preparation of electrocompetent cells: An overnight pre-culture of *E. coli* NEB® 5-alpha Competent *E. coli* (high efficiency) or *E. coli* LCB3063 is diluted to a final $OD_{600} = 0.05$ into 100 mL of LB medium and cultured at 37 °C until reaching $OD_{600} = 0.9$. The growth is, then, stopped by chilling the cells at 4 °C on ice for 40 min. Bacterial cells are harvested by centrifugation at 4000 *g* for 10 min and re-suspended in 100 mL of sterile MilliQ water + 10% glycerol. This washing step is repeated two times, reducing the volume of the washes to 50 mL and 30 mL, respectively. Finally, bacterial cells are resuspended in sterile MilliQ water + 10% glycerol to obtain a final concentration between 4 and 6×10^{10} cells/mL. Cells are aliquoted and stored at −80 °C.

Protein spin labeling: Prior to spin labeling, 100 nmol of protein are treated with an excess of DTT (20x) at 4 °C for 30 min to reduce the cysteine moieties, then removed by PD10 desalting column (GE Healthcare), against Tris·HCl 10 mM pH 7.4 buffer. The factions containing the protein are pooled and incubated with MA-Proxyl nitroxide a ten- or 20-fold molar excess proteins containing one or two cysteine residues, respectively. A second PD10 desalting column against the same buffer described above is performed to remove the excess of unbound spin label. The collected fractions are, then, checked by EPR spectroscopy and polished by centrifugation in 2 mL Vivaspin concentrators 10 kDa MWCO (Sartorius) 7500 *g* 5 min each. The concentration of the labeled protein is evaluated by measuring the OD at 280 nm. The labeling yield was 80–100% singly labeled NarJ variants; 185–200% doubly labeled NarJ variants.

Protein labeling with fluorescent tags: For protein labeling with fluorescent labels we used Cyanine5 NHS ester or sCyanine5 NHS ester, both purchased from Lumiprobe. The labeling protocol employed for the 2 fluorophores was the same. A solution of NarJwt (100 nmol) in PBS 0.1 M pH 8.1 was incubated with Cyanine or sCyanine5 NHS ester fluorophore in fourfold excess for 16 h at 4 °C. Then, the reaction mixture underwent several rounds of centrifugation (13000 *g*, 10 min, 4 °C) in order to pellet and remove the precipitated fluorophore while keeping the supernatant (containing the protein). Once no more pellet was detectable after centrifugation, gel filtration (using PD10 desalting column, GE Healthcare) against Tris·HCl 10 mM pH 7.4 buffer was performed in order to remove the excess of unreacted fluorophore. The fractions are concentrated and diluted 4 times using Sartorius 2 mL centrifugal units (MWCO 10 kDa). The concentrated pool is loaded in a PD10 desalting column against and the bright blue fractions are, again, polished by concentration as mentioned before. To fully washout the leftover of unreacted dye we checked the flow through absorption (at 646 nm) and thus to know when stopping washing the sample.

The labeling ratio was calculated from the ratio of the measured absorbance of the label at 646 nm (using the extinction coefficient $\varepsilon = 250000\,M^{-1}cm^{-1}$) and the absorbance of protein at 280 nm (using the extinction coefficient $\varepsilon = 21430\,M^{-1}cm^{-1}$), corrected by the absorption of the dye at 280 nm. The labeling ratio was evaluated to be between 5 and 5.5 dyes per NarJ protein.

In-cell protein delivery: Electrocompetent *E. coli* cells (20 μL), prepared as indicated before are incubated with an equal amount of labeled protein solution, during 10 min on ice. In our study, protein stock concentration was between 800 μM and 1 mM. The protein cell mixture is, then, transferred into a pre-chilled 1 mm-gap cuvette (VRW) and electroporated. All the experiments were performed with a BioRad Gene Pulser Xcell Electroporation Systems using the following parameters: voltage = 1800 V, resistance = 200 ohm, impulse = single. After the electric pulse, the cells membrane integrity is recovered by addiction of 500 μL of Super Optimal broth with Catabolite repression (SOC, NEB). Cells are then washed 3 times by centrifugation at 3200 *g*, 2 min, 4 °C.

In the first wash, the pellet is resuspended in 500 μL of PBS 10 mM pH 7.5, + 0.005% Triton solution; in the other washing steps, PBS 10 mM, pH 7.5 is in general used. In order to check that the washing cycles are enough to remove any not delivered protein in the sample, the cells were pelleted and the supernatant is checked by EPR analysis (Figure S3). This step is in general repeated for an appropriate number of times, at least till the absence of an EPR signal in the supernatant. After the last washing cycle, cells are resuspended in 50 μL of PBS 10 mM pH 7.5, and 1% low temperature melting agarose (Euromedex) and transferred in an EPR capillary. The time between the preparation of the "in-cell" sample and the beginning of EPR spectra acquisition was about 10–15 min.

Laser scanning confocal microscopy: Confocal images have been acquired using a laser scanning microscope (Zeiss LSM 880 with Airyscan, RRID:SCR_020925) using a Plan-Apochromat 63x/1.4 Oil DIC M27 objective. Acquisitions have been performed in Airyscan mode, with a pinhole size of 1.18 to 1.87 Airy units, using a 633 nm laser and a long pass filter (LP 645) to excite and detect NarJ-Cy5 or NarJ-sCy5 fluorescence. Typically, images were 800 × 800 pixels, with a pixel physical size of 44–70 nm and with a separation between Z planes of 200 to 300 nm. Transmission images were acquired using Differential Interference Contrast (DIC) microscopy. For imaging, 1 μL of bacteria was spot on a #1.5 microscope coverslip (CG15XH1, Thorlabs) and hold on place using an agar pad (1% *w/v* agarose in LB medium). Images have been analyzed using FIJI[42] (RRID:SCR_002285). Rough Airyscan images have been processed with the FIJI plugin *AiryscanJ*[43] using the ISM reconstruction method.

Fluorescence monitoring by flow cytometry: In flow cytometry experiments we used NarJ labeled with the fluorophore ATTO-488 (Lumiprobe). *E. coli* cells samples (10^{-2}) were analyzed using flow cytometry (A50-micro instrument Apogee Flow Systems, UK) equipped with an argon ion laser (Asbly, $\lambda_{ex} = 488$ nm, 50 mV) and specific fluorescence filter set (Green (Gn): 535/35 nm, Orange (Or): 585/20 nm and Red (Rd): > 610 nm). Calibration beads (Apogee Flow Systems, 1 μm, $\lambda_{ex} = 488$ nm and a broad fluorescence

emission in the Gn, Or and Rd channels, 5000 events × μL^{-1}) were used as a standard to ensure the quality of the analysis. Each sample was run using the following setting: constant sample flow rate; sheath pressure 200 mbar; photodetector voltages for small and large angle light scatter, Gn, Or, Red fluorescence channels were respectively fixed at 200, 275, 700, 518 and 550 V. Data were acquired in log scale using PC control v3.40 and histogram v110.0 software (Apogee Flow Systems) and analyzed with the FlowJoV10 software (TreeStarInc.). The small versus large angle light scatter color plot was used to discriminate bacterial populations from the background noise. Then, fluorescence intensities gated on the bacterial populations were compared. As far as fluorescence intensity was concerned, bi-exponential representation was used. This display consists in a data transformation in order to use a linear scale to display low signals (intensities close to the origin) and a logarithmic scale for the larger ones (intensities from 10 to 10000). This is a "Logicle" display method widely accepted by cytometrics that avoids deceptive effects of logarithmic scaling for low signals and compensated data in flow cytometry. Gating discriminating fluorescents from non-fluorescents sub-populations was made and data were exported to Excel software to make further statistical analyses.[44]

In-cell nitrate reductase activity assay: In-cell delivery of the NarJ protein was performed using the protocol described above using electrocompetent JC4023 cells transformed with either of the plasmids. As a negative control for in-cell protein delivery, electrocompetent cells were subjected to electroporation with deionized water. After electroporation, cells were subjected to several washing steps in PBS buffer, transferred in an anaerobic glovebox (95% N_2, 5% H_2) and resuspended in 25 μL of PBS buffer previously degassed. Benzyl viologen-nitrate reductase activity was measured spectrophotometrically at 604 nm as previously described by following the oxidation of reduced benzyl viologen (i.e., BV) concomitant with the reduction of nitrate to nitrite.[29] The sample is transferred in a plastic cuvette filled with 1 mL of PBS buffer supplemented with 0.05 mM dithionite and 1.5 mM BV. When the absorbance is stable, 25 μL of cells suspension is added. After waiting the stabilization of the absorbance, 1 mM of substrate (KNO_3) is added to the solution. The slope after the addition of the substrate is then normalized for the extinction coefficient of the BV (7400 $M^{-1} cm^{-1}$) and for the number of cells incubated with the protein before dilution in cells/mL.

Cell lysates preparation: Cell pellets from an *E. coli* DH5a culture (3 L final OD 0.9) were frozen overnight, thawed and resuspended in 1 mL of buffer (20 mM KH_2PO_4, 50 mM NaCl, pH 6.0) containing a few crystals of DNase. Cell lysis was completed by sonication and the lysate was centrifuged at 20000 g for 30 min and flash frozen in liquid nitrogen. Cell lysates were prepared by using the same cell strain at the same growth stage of the cells used for in-whole-cells EPR experiments. The concentration of cell lysates was in the range 0.5–0.7 g/mL. To avoid dilution of the lysates, the samples for EPR analysis were prepared by adding 2 μL of labeled protein to a volume of 50 μL of cell lysate, with a final spin concentration of 40 μM.

CW EPR: All the room temperature CW-EPR experiments are recorded on a spectrometer Elexsys 500 Bruker equipped with a Super High Q sensitivity resonator operating at X band (9.9 GHz) at room temperature. Samples are injected in a quartz capillary whose sensible volume was 40 μL.

The parameters used are the following: microwaves power = 10 mW; magnetic field modulation amplitude = 1 G; field sweep = 150 G; receiver gain = 60 dB. In the case of kinetics recording the field sweep is reduced at 100 G and the delay between each acquisition is 8.1 s. The spin concentration is calculated from the double integration of the CW EPR spectrum at room temperature and under non-saturating conditions and compared with that given for a MTSL nitroxide sample of a known concentration. In the case of EPR recording over time, the number of cells as starting point was 4–7 × 10^{10} cells/mL as calculated from OD_{600} measurements.

EPR spectra were simulated with the 'Slow Motion' mode of SimLabel,[25] a GUI of EasySpin.[26] The EasySpin function used for spectra simulation was "chili", while the used routine is described here.[25]

DEER experiments: DEER distance measurements were performed at 60 K, on a Bruker ELEXSYS E580 spectrometer equipped with an Oxford helium temperature regulation unit, at Q-band using the standard EN 5107D2 resonator. All the measurements were performed at 60 K on 20 μL of sample loaded into quartz capillaries and flash frozen in liquid nitrogen. The DEER traces were, then, analyzed using DeerAnalysis2019 software (http://www.epr.ethz.ch/software/index Jeschke G. 2011. DeerAnalysis. ETH, Zürich, Switzerland).

Acknowledgements

The authors are grateful for access to the EPR facilities at the French Research Infrastructure INFRANALYTICS (FR2054) and the Aix-Marseille University EPR center. We also acknowledge the Microscopy and Scientific Imaging (MISc) facility at the CRCM (Marseille, France) for confocal imaging. We acknowledge financial support from the "Agence Nationale de la Recherche" (ANR-18-CE11-0007-01) and from the "Conseil Régional Région Sud" (A.P. PhD Fellowship EJD-2018-2021). The project leading to this publication has received funding from the A*Midex Foundation of Aix-Marseille University, funded by socio-economic partners.

Conflict of Interests

There are no conflicts to declare.

Data Availability Statement

The data that support the findings of this study are available from the corresponding author upon reasonable request.

Keywords: EPR spectroscopy · in-cell studies · nitroxide labels · protein structural dynamics · site-directed spin labeling

[1] J. M. Plitzko, B. Schuler, P. Selenko, *Curr. Opin. Struct. Biol.* **2017**, *46*, 110–121.
[2] a) Y. Kadan, F. Tollervey, N. Varsano, J. Mahamid, A. Gal, *Proc. Natl. Acad. Sci. USA* **2021**, *118*, e2025670118; b) N. Groysbeck, M. Donzeau, A. Stoessel, A.-M. Haeberle, S. Ory, D. Spehner, P. Schultz, O. Ersen, M. Bahri, D. Ihiawakrim, G. Zuber, *Nanoscale Adv.* **2021**, *3*, 6940–6948.
[3] A. Graziadei, J. Rappsilber, *Structure* **2022**, *30*, 37–54.
[4] a) Y. Bousmah, H. Valenta, G. Bertolin, U. Singh, V. Nicolas, H. Pasquier, M. Tramier, F. Merola, M. Erard, *ACS Sens.* **2021**, *6*, 3940–3947; b) C. S. Ziegler, L. Bouchab, M. Tramier, D. Durand, F. Fieschi, S. Dupré-Crochet, F. Mérola, O. Nüße, M. Erard, *J. Biol. Chem.* **2019**, *294*, 3824–3836.

[5] M. Paloni, R. Bailly, L. Ciandrini, A. Barducci, *J. Phys. Chem. B* **2020**, *124*, 9009–9016.
[6] a) E. Luchinat, M. Cremonini, L. Banci, *Chem. Rev.* **2022**, *122*, 9267–9306; b) F.-X. Theillet, *Chem. Rev.* **2022**, *122*, 9497–9570; c) R. Ghosh, Y. Xiao, J. Kragelj, K. K. Frederick, *J. Am. Chem. Soc.* **2021**, *143*, 18454–18466.
[7] A. Bonucci, O. Ouari, B. Guigliarelli, V. Belle, E. Mileo, *ChemBioChem* **2020**, *21*, 451–460.
[8] R. Igarashi, T. Sakai, H. Hara, T. Tenno, T. Tanaka, H. Tochio, M. Shirakawa, *J. Am. Chem. Soc.* **2010**, *132*, 8228–8229.
[9] a) P. Roser, M. J. Schmidt, M. Drescher, D. Summerer, *Org. Biomol. Chem.* **2016**, *14*, 5468–5476; b) M. Martinho, E. Fournier, N. Le Breton, E. Mileo, V. Belle in *Electron Paramagnetic Resonance, Vol. 26*, The Royal Society of Chemistry, **2019**, pp. 66–88.
[10] Y. Yang, S.-N. Chen, F. Yang, X.-Y. Li, A. Feintuch, X.-C. Su, D. Goldfarb, *Proc. Natl. Acad. Sci. USA* **2020**, *117*, 20566–20575.
[11] a) G. Karthikeyan, A. Bonucci, G. Casano, G. Gerbaud, S. Abel, V. Thomé, L. Kodjabachian, A. Magalon, B. Guigliarelli, V. Belle, O. Ouari, E. Mileo, *Angew. Chem. Int. Ed.* **2018**, *57*, 1366–1370; *Angew. Chem.* **2018**, *130*, 1380–1384; b) S. Bleicken, T. E. Assafa, H. Zhang, C. Elsner, I. Ritsch, M. Pink, S. Rajca, G. Jeschke, A. Rajca, E. Bordignon, *ChemistryOpen* **2019**, *8*, 1057–1065; c) N. Fleck, C. A. Heubach, T. Hett, F. R. Haege, P. P. Bawol, H. Baltruschat, O. Schiemann, *Angew. Chem. Int. Ed.* **2020**, *59*, 9767–9772; *Angew. Chem.* **2020**, *132*, 9854–9859; d) Y. Yang, F. Yang, Y.-J. Gong, T. Bahrenberg, A. Feintuch, X.-C. Su, D. Goldfarb, *J. Phys. Chem. Lett.* **2018**, *9*, 6119–6123; e) Y. Yang, F. Yang, X.-Y. Li, X.-C. Su, D. Goldfarb, *J. Phys. Chem. B* **2019**, *123*, 1050–1059; f) S. Ketter, A. Gopinath, O. Rogozhnikova, D. Trukhin, V. M. Tormyshev, E. G. Bagryanskaya, B. Joseph, *Chem. Eur. J.* **2021**, *27*, 2299–2304.
[12] a) M. J. Schmidt, J. Borbas, M. Drescher, D. Summerer, *J. Am. Chem. Soc.* **2014**, *136*, 1238–1241; b) L. Galazzo, G. Meier, M. H. Timachi, C. A. J. Hutter, M. A. Seeger, E. Bordignon, *Proc. Natl. Acad. Sci. USA* **2020**, *117*, 2441–2448; c) P. Widder, J. Schuck, D. Summerer, M. Drescher, *Phys. Chem. Chem. Phys.* **2020**, *22*, 4875–4879.
[13] a) Y. Yang, B.-B. Pan, X. Tan, F. Yang, Y. Liu, X.-C. Su, D. Goldfarb, *J. Phys. Chem. Lett.* **2020**, *11*, 1141–1147; b) S. Kucher, C. Elsner, M. Safonova, S. Maffini, E. Bordignon, *J. Phys. Chem. Lett.* **2021**, *12*, 3679–3684; c) J. J. Jassoy, A. Berndhäuser, F. Duthie, S. P. Kühn, G. Hagelueken, O. Schiemann, *Angew. Chem. Int. Ed.* **2017**, *56*, 177–181; *Angew. Chem.* **2017**, *129*, 183–187; d) A. Collauto, S. von Bülow, D. B. Gophane, S. Saha, L. S. Stelzl, G. Hummer, S. T. Sigurdsson, T. F. Prisner, *Angew. Chem. Int. Ed.* **2020**, *59*, 23025–23029; *Angew. Chem.* **2020**, *132*, 23225–23229.
[14] a) S. Brandon, A. H. Beth, E. J. Hustedt, *J. Magn. Reson.* **2012**, *218*, 93–104; b) O. Schiemann, C. A. Heubach, D. Abdullin, K. Ackermann, M. Azarkh, E. G. Bagryanskaya, M. Drescher, B. Endeward, J. H. Freed, L. Galazzo, D. Goldfarb, T. Hett, L. Esteban Hofer, L. Fábregas Ibáñez, E. J. Hustedt, S. Kucher, I. Kuprov, J. E. Lovett, A. Meyer, S. Ruthstein, S. Saxena, S. Stoll, C. R. Timmel, M. Di Valentin, H. S. McHaourab, T. F. Prisner, B. E. Bode, E. Bordignon, M. Bennati, G. Jeschke, *J. Am. Chem. Soc.* **2021**, *143*, 17875–17890; c) M. Pannier, S. Veit, A. Godt, G. Jeschke, H. W. Spiess, *J. Magn. Reson.* **2000**, *142*, 331–340; d) D. Goldfarb, *J. Magn. Reson.* **2019**, *306*, 102–108.
[15] a) W. L. Hubbell, H. S. McHaourab, C. Altenbach, M. A. Lietzow, *Structure* **1996**, *4*, 779–783; b) W. L. Hubbell, C. J. Lopez, C. Altenbach, Z. Yang, *Curr. Opin. Struct. Biol.* **2013**, *23*, 725–733; c) N. Le Breton, M. Martinho, E. Mileo, E. Etienne, G. Gerbaud, B. Guigliarelli, V. Belle, *Front. Mol. Biosci.* **2015**, *2*, 21.
[16] J. L. Sarver, M. Zhang, L. Liu, D. Nyenhuis, D. S. Cafiso, *Biochemistry* **2018**, *57*, 1045–1053.
[17] a) J. Cattani, V. Subramaniam, M. Drescher, *Phys. Chem. Chem. Phys.* **2017**, *19*, 18147–18151; b) F. Torricella, A. Bonucci, P. Polykretis, F. Cencetti, L. Banci, *Biochem. Biophys. Res. Commun.* **2021**, *570*, 82–88; c) K. Singewald, M. J. Lawless, S. Saxena, *J. Magn. Reson.* **2019**, *299*, 21–27.
[18] B. Joseph, A. Sikora, D. S. Cafiso, *J. Am. Chem. Soc.* **2016**, *138*, 1844–1847.
[19] J. Jumper, R. Evans, A. Pritzel, T. Green, M. Figurnov, O. Ronneberger, K. Tunyasuvunakool, R. Bates, A. Žídek, A. Potapenko, A. Bridgland, C. Meyer, S. A. A. Kohl, A. J. Ballard, A. Cowie, B. Romera-Paredes, S. Nikolov, R. Jain, J. Adler, T. Back, S. Petersen, D. Reiman, E. Clancy, M. Zielinski, M. Steinegger, M. Pacholska, T. Berghammer, S. Bodenstein, D. Silver, O. Vinyals, A. W. Senior, K. Kavukcuoglu, P. Kohli, D. Hassabis, *Nature* **2021**, *596*, 583–589.
[20] T. D. Nilaweera, D. A. Nyenhuis, D. S. Cafiso, *eLife* **2021**, *10*.
[21] A. Gopinath, B. Joseph, *Angew. Chem. Int. Ed.* **2022**, *61*, e202113448.
[22] a) F. Blasco, J. P. Dos Santos, A. Magalon, C. Frixon, B. Guigliarelli, C. L. Santini, G. Giordano, *Mol. Microbiol.* **1998**, *28*, 435–447; b) A. Vergnes, J. Pommier, R. Toci, F. Blasco, G. Giordano, A. Magalon, *J. Biol. Chem.* **2006**, *281*, 2170–2176; c) P. Lanciano, A. Vergnes, S. Grimaldi, B. Guigliarelli, A. Magalon, *J. Biol. Chem.* **2007**, *282*, 17468–17474.
[23] a) S. Zakian, D. Lafitte, A. Vergnes, C. Pimentel, C. Sebban-Kreuzer, R. Toci, J. B. Claude, F. Guerlesquin, A. Magalon, *FEBS J.* **2010**, *277*, 1886–1895; b) M. Lorenzi, L. Sylvi, G. Gerbaud, E. Mileo, F. Halgand, A. Walburger, H. Vezin, V. Belle, B. Guigliarelli, A. Magalon, *PLoS One* **2012**, *7*, e49523.
[24] D. C. Bay, C. S. Chan, R. J. Turner, *BMC Evol. Biol.* **2015**, *15*, 110.
[25] E. Etienne, N. Le Breton, M. Martinho, E. Mileo, V. Belle, *Magn. Reson. Chem.* **2017**, *55*, 714–719.
[26] S. Stoll, A. Schweiger, *J. Magn. Reson.* **2006**, *178*, 42–55.
[27] a) R. Crawford, J. P. Torella, L. Aigrain, A. Plochowietz, K. Gryte, S. Uphoff, A. N. Kapanidis, *Biophys. J.* **2013**, *105*, 2439–2450; b) M. Sustarsic, A. Plochowietz, L. Aigrain, Y. Yuzenkova, N. Zenkin, A. Kapanidis, *Histochem. Cell Biol.* **2014**, *142*, 113–124.
[28] A. Magalon, M. Asso, B. Guigliarelli, R. A. Rothery, P. Bertrand, G. Giordano, F. Blasco, *Biochemistry* **1998**, *37*, 7363–7370.
[29] R. W. Jones, P. B. Garland, *Biochem. J.* **1977**, *164*, 199–211.
[30] H. Yan, W. Huang, C. Yan, X. Gong, S. Jiang, Y. Zhao, J. Wang, Y. Shi, *Cell Rep.* **2013**, *3*, 716–723.
[31] G. Rivas, A. P. Minton, *Trends Biochem. Sci.* **2016**, *41*, 970–981.
[32] A. J. Guseman, G. M. P. Goncalves, S. L. Speer, G. B. Young, G. J. Pielak, *Proc. Natl. Acad. Sci. USA* **2018**, *115*, 10965–10970.
[33] B. D. Bennett, E. H. Kimball, M. Gao, R. Osterhout, S. J. Van Dien, J. D. Rabinowitz, *Nat. Chem. Biol.* **2009**, *5*, 593–599.
[34] M. Sarkar, J. Lu, G. J. Pielak, *Biochemistry* **2014**, *53*, 1601–1606.
[35] S. L. Speer, C. J. Stewart, L. Sapir, D. Harries, G. J. Pielak, *Ann. Rev. Biophys.* **2022**, *51*, 267–300.
[36] A. A. M. André, E. Spruijt, *Int. J. Mol. Sci.* **2020**, *21*, 5908.
[37] a) A. P. Jagtap, I. Krstic, N. C. Kunjir, R. Hansel, T. F. Prisner, S. T. Sigurdsson, *Free Radical Res.* **2015**, *49*, 78–85; b) S. Huang, H. Zhang, J. T. Paletta, S. Rajca, A. Rajca, *Free Radical Res.* **2018**, *52*, 327–334.
[38] a) B. Mateos, M. Sealey-Cardona, K. Balazs, J. Konrat, G. Staffler, R. Konrat, *Angew. Chem. Int. Ed.* **2020**, *59*, 3886–3890; *Angew. Chem.* **2020**, *132*, 3914–3918; b) K. Inomata, H. Kamoshida, M. Ikari, Y. Ito, T. Kigawa, *Chem. Commun.* **2017**, *53*, 11245–11248.
[39] a) Y. Yang, F. Yang, Y. J. Gong, J. L. Chen, D. Goldfarb, X. C. Su, *Angew. Chem. Int. Ed.* **2017**, *56*, 2914–2918; *Angew. Chem.* **2017**, *129*, 2960–2964; b) G. Prokopiou, M. D. Lee, A. Collauto, E. H. Abdelkader, T. Bahrenberg, A. Feintuch, M. Ramirez-Cohen, J. Clayton, J. D. Swarbrick, B. Graham, G. Otting, D. Goldfarb, *Inorg. Chem.* **2018**, *57*, 5048–5059.
[40] C. Li, G.-F. Wang, Y. Wang, R. Creager-Allen, E. A. Lutz, H. Scronce, K. M. Slade, R. A. S. Ruf, R. A. Mehl, G. J. Pielak, *J. Am. Chem. Soc.* **2010**, *132*, 321–327.
[41] M. Pepelnjak, N. de Souza, P. Picotti, *Trends Biochem. Sci.* **2020**, *45*, 919–920.
[42] J. Schindelin, I. Arganda-Carreras, E. Frise, V. Kaynig, M. Longair, T. Pietzsch, S. Preibisch, C. Rueden, S. Saalfeld, B. Schmid, J. Y. Tinevez, D. J. White, V. Hartenstein, K. Eliceiri, P. Tomancak, A. Cardona, *Nat. Methods* **2012**, *9*, 676–682.
[43] S. Prigent, S. Dutertre, C. Kervrann in *ICASSP 2020–2020 IEEE International Conference on Acoustics, Speech and Signal Processing (ICASSP)*, **2020**, pp. 1075–1079.
[44] D. R. Parks, M. Roederer, W. A. Moore, *Cytom. Part. J. Int. Soc. Anal. Cytol.* **2006**, *69*, 541–551.
[45] F. Torricella, A. Pierro, E. Mileo, V. Belle, A. Bonucci, *Proteins and Proteomics* **2021**, *1869 (7)*, 140653, DOI: 10.1016/j.bbapap.2021.140653.
[46] C. J. López, S. Oga, W. L. Hubbell, *Biochemistry* **2012**, *51*, 6568–6583.
[47] A. D. Freeman, J. J. et al., *Biochemistry* **2016**, *55*, 4166–4172.
[48] V. Belle et al., *Biochemistry* **2007**, *46*, 2205–2214.

Manuscript received: July 18, 2022
Accepted manuscript online: October 6, 2022
Version of record online: October 31, 2022